# NEAR-FIELD MAGNETIC DIPOLE MOMENT ANALYSIS

*Patrick K. Harris, ManTech Aerospace Technology Applications Center*

## Biography

*Patrick K. Harris, P.E., NCE*
Mr. Harris was born in Cheverly, Md. in 1967. He received a B.S. in nuclear/electrical engineering from University of Maryland, College Park in 1990 and a M.S. in engineering management from Kennedy-Western University, Cheyenne, Wyo. in 1999. Currently, he is a test engineer for ManTech Aerospace Technology Applications Center, at NASA's Goddard Space Flight Center (GSFC) in Greenbelt, Md. Mr. Harris worked for the University of Maryland Department of Environmental Safety in 1993 and from 1989-1990, and Bechtel Power Corporation from 1990-1993. He holds a Maryland Professional Engineer license, NARTE EMC Engineer certification and is a Senior Member of IEEE.

## Abstract

This paper describes the data analysis technique used for magnetic testing at the NASA Goddard Space Flight Center (GSFC). Excellent results have been obtained using this technique to convert a spacecraft's measured magnetic field data into its respective magnetic dipole moment model. The model is most accurate with the earth's geomagnetic field cancelled in a spherical region bounded by the measurement magnetometers with a minimum radius large enough to enclose the magnetic source. Considerably enhanced spacecraft magnetic testing is offered by using this technique in conjunction with a computer-controlled magnetic field measurement system. Such a system, with real-time magnetic field display capabilities, has been incorporated into other existing magnetic measurement facilities and is also used at remote locations where transport to a magnetics test facility is impractical.

## Keywords

Data Acquisition, Data Analysis, Environmental Testing, Magnetics, Modeling and Simulation of Environments, and Optimizing Environmental Test Techniques.

## Introduction

A spacecraft whose magnetic field has been accurately calibrated possesses a unique capability for acquiring magnetic field and other scientific data. Geomagnetic, as well as planetary and interplanetary magnetic measurements depend on such a controlled spacecraft magnetic environment for accurate results. To provide this environment, restraint of magnetic materials on board the spacecraft and sophisticated prelaunch magnetic tests are required. Some facilities, like the GSFC Spacecraft Magnetic Test Facility (SMTF), are able to null Earth's geomagnetic field to less than 0.5 nT, providing a controlled environment for measurement and control of spacecraft fields.

The magnetic field modeling technique described herein was developed at the Goddard Magnetic Test Facility as an aid in the evaluation of spacecraft magnetic fields and has been used for over thirty years. Three specific problem areas requiring magnetic field measurements have been investigated using this technique:

- Spacecraft attitude control problems resulting from a large intrinsic magnetic dipole moment;
- Reduced accuracy of data returned from magnetometer experiments due to spacecraft bias fields; and
- Complicated data analysis caused by spacecraft magnetic fields around low-energy electron experiments.

The magnetic field modeling technique described in this paper, combined with a computer measurement system, provides a means of solving the above problems. Using the computerized modeling technique to provide a near-real-time visual representation of the spacecraft magnetic field reduces testing time required for complex magnetic measurements. This visual representation also aids in reduction of the dipole moment by showing the correct orientation for placement of compensation magnets or demagnetization treatment. In addition, the magnetic field modeling technique provides a rigorous method of determining the magnetic field at any point of interest around the spacecraft, based upon a limited number of measurements at discrete points. This enables a rapid and comprehensive evaluation of spacecraft magnetic fields for the solution of magnetometer bias and low-energy electron deflection problems.

# Background

In 1972, William L. Eichhorn published a NASA technical report describing a dipole moment measurement technique using near-field magnetic data [1]. The technique assumes that a spacecraft's magnetic field can be represented by the addition of a number of multi-pole fields. These fields are measured in the near-field region that begins on a spherical surface, which totally encloses the magnetic source and extends outward until the fields become dipolar. Near-field analysis allows dipole moment data to be taken closer to the spacecraft where magnetic fields are strong enough for reliable measurements. The technique has been used with good results at the Goddard Magnetic Test Facility for magnetic testing of various spacecraft.

A typical spacecraft orientation for magnetic testing is shown in Figure 1 (where $\omega$ = direction around axis of rotation). Four tri-axial magnetometers are located along one of the spacecraft axes, and magnetic field data is acquired while rotating the spacecraft about the vertical (Z) axis past an array of fixed magnetometer probes. The equations for calculating the magnetic fields present at the X-, Y-, and Z-axes of a magnetometer sensor located a distance R from the center of the spacecraft (as a function of rotational angle $\theta$) were derived in [1]. With a few minor changes in notation and truncation of the infinite series at n = 4, to provide a finite series for modeling purposes, these magnetic field equations become:

$$B_x(R,\theta,0) = \sum_{n=1}^{4}\sum_{m=0}^{n}(n+1)/R^{n+2}\left(A_{nm}\cos m\theta + B_{nm}\sin m\theta\right)P_n^m(0)$$

$$B_y(R,\theta,0) = \sum_{n=1}^{4}\sum_{m=0}^{n}m/R^{n+2}\left(A_{nm}\sin m\theta + B_{nm}\cos m\theta\right)P_n^m(0)$$

$$B_z(R,\theta,0) = \sum_{n=1}^{4}\sum_{m=0}^{n}1/R^{n+2}\left(A_{nm}\cos m\theta + B_{nm}\sin m\theta\right)\partial/\partial\phi\left(P_n^m(0)\right)$$

Where:

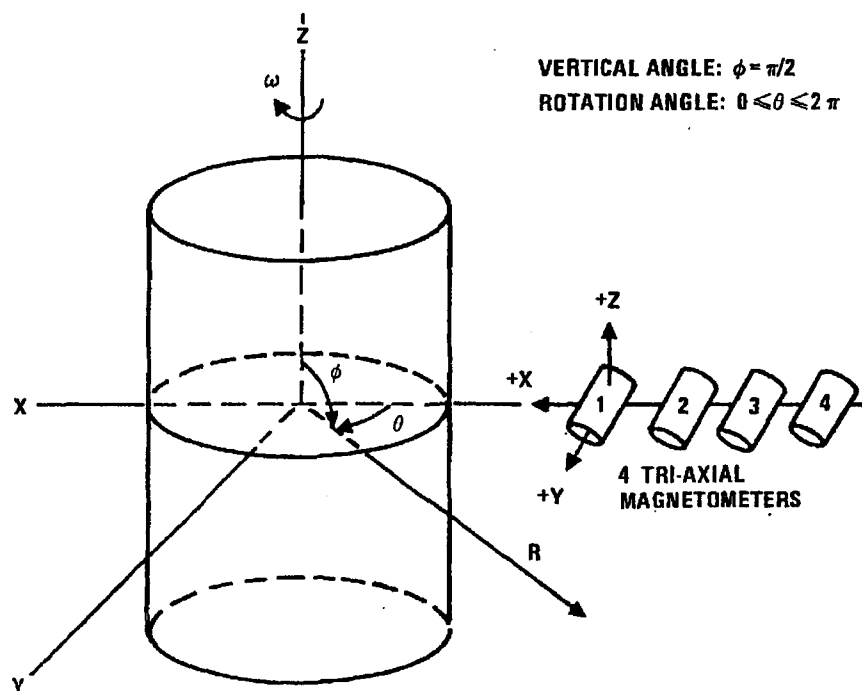| | |
|---|---|
| $B_x(R,\theta,0)$ = | magnetic field component (nT) along X magnetometer axis as a function of R and $\theta$; |
| R      = | radial distance from center of magnetic mass to magnetometer, which must be greater than maximum radius of the magnetic source in meters (m); |
| $A_{nm}$, $B_{nm}$ = | multi-pole moment coefficients; |
| $\theta$      = | rotation angle (0 to $2\pi$); |
| $P_n^m(0)$   = | associated Legendre functions of P (cos $\varphi$) where $\varphi = \pi/2$; and |
| $\varphi$      = | vertical angle with respect to spacecraft axis of rotation. |



Figure 1. Spacecraft Orientation for Magnetic Testing

In 1973, the magnetic field modeling technique was developed by Thomas N. Roy to extend near-field analysis. The technique is capable of producing accurate mathematical models from the same near-field analysis data. Near-field analysis involves only the cos $\theta$ and sin $\theta$ terms of the above equations for calculation of X- and Y-axis dipole moments, and the constant term with respect to $\theta$ for the Z-axis moment. Extension of near-field analysis for magnetic field modeling involves as many as eight harmonic terms of the magnetic field equations. Experience in using these equations to model fields around several different spacecraft has shown a solution order of n = 4 to be sufficient for accurate modeling over regions of interest. The technique can easily be extended to higher ordered harmonics for modeling the extreme near-field regions of strongly multi-polar sources.

This paper describes the magnetic field modeling technique and its application to spacecraft magnetic fields. Limitations of this technique, as well as other possible uses, are discussed at the end of the paper.

## Magnetic Field Modeling

Results obtained from solution of the magnetic field equations for n = 1 to 4 indicate that the magnetic field of a spacecraft can be described anywhere on a plane containing the measurement magnetometers by:

$$B_j(R,\theta) = DC_j / R^{A_j} + \sum_{n=1}^{4}(C_j n)\cos(n\theta) / R^{Bn_j} + \sum_{n=1}^{4}(S_j n)\sin(n\theta) / R^{Cn_j}$$

Where:

| | | |
|---|---|---|
| j | = | measurement magnetometer axes X, Y or Z; |
| R | = | radial distance; |
| $\theta$ | = | rotational angle with respect to magnetometer axes; |
| n | = | order of Fourier solution usually truncated after eight terms; |
| $DC_j$ | = | constant field (with respect to $\theta$) modeling coefficient calculated for each axis; |
| $C_j n$ | = | cosine field modeling coefficient calculated for each axis and n = 1 to 4; |
| $S_j n$ | = | sine field modeling coefficient calculated for each axis and n = 1 to 4; |
| $A_j$ | = | constant field decay power calculated for each axis; |
| $Bn_j$ | = | cosine field decay power calculated for each axis and n = 1 to 4; and |
| $Cn_j$ | = | sine field decay power calculated for each axis and n = 1 to 4. |

Therefore, to construct a magnetic field model using the above equation, a method is needed to calculate the field modeling coefficients and field decay powers.

The procedure for calculating field modeling coefficients and field decay powers begins with this fourth-order Fourier analysis. The analysis produces eight Fourier coefficients for each axis (j) (four for the Z-axis) of every magnetometer (i), and their standard deviations. Fourier coefficients typically represent averaged values for five spacecraft rotations.

Four cosine Fourier coefficients, calculated for n = 1 to 4:

$$C_j n_i = \tfrac{1}{\pi}\sum_{\theta=0}^{2\pi} B_{ji}(R_i,\theta)\cos(n\theta)$$

Four sine Fourier coefficients, calculated for n = 1 to 4:

$$S_j n_i = \tfrac{1}{\pi}\sum_{\theta=0}^{2\pi} B_{ji}(R_i,\theta)\sin(n\theta)$$

Constant Fourier coefficient:

$$DC_{ji} = \tfrac{1}{2\pi}\sum_{\theta=0}^{2\pi} B_{ji}(R_i,\theta)$$

Where:

| | | |
|---|---|---|
| i | = | magnetometer number, 1 to 4; |
| $B_{ji}(R_i,\theta)$ = | | rotational magnetic field; and |
| j | = | magnetometer axes X, Y, or Z. |

Next, dividing them by their respective Fourier coefficients normalizes the standard deviations. The normalized cosine standard deviations, calculated for n = 1 to 4 are:

$$\sigma_n C_j n_i = \sigma C_j n_i / C_j n_i$$

The normalized sine standard deviations, calculated for n = 1 to 4 are:

$$\sigma_n S_j n_i = \sigma S_j n_i / S_j n_i$$

The normalized constant (Z-axis) standard deviation is:

$$\sigma_n DC_{ji} = \sigma DC_{ji} / DC_{ji}$$

At this point, the technique assumes that for each axis (j) and each order of Fourier analysis (n), the Fourier coefficients from each magnetometer have the same polarity and decrease with increasing radius (R). This permits the calculation of field decay powers for each order of Fourier analysis starting with the constant term. All possible combinations between the four magnetometers are averaged. Each combination is weighted using the normalized standard deviations calculated above:

$A_j$ = constant field decay power;
$Bn_j$ = cosine field decay power calculated for n = 1 to 4; and
$Cn_j$ = sine field decay power calculated for n = 1 to 4.

For example, using DC Fourier coefficients and four magnetometers, where $R_1$, $R_2$, $R_3$, and $R_4$ are the actual magnetometer radii from the center of rotation, calculating the constant field decay power:

$$(A_j)_{1,2} = \log[(DC_{j1})/(DC_{j2})]/\log(R_1/R_2)$$
$$(A_j)_{1,3} = \log[(DC_{j1})/(DC_{j2})]/\log(R_1/R_3)$$
$$(A_j)_{1,4} = \log[(DC_{j1})/(DC_{j4})]/\log(R_1/R_4)$$
$$(A_j)_{2,3} = \log[(DC_{j2})/(DC_{j3})]/\log(R_2/R_3)$$
$$(A_j)_{2,4} = \log[(DC_{j2})/(DC_{j4})]/\log(R_2/R_4)$$
$$(A_j)_{3,4} = \log[(DC_{j3})/(DC_{j4})]/\log(R_3/R_4)$$

The averaged field decay power is thus:

$$A_j = \frac{\begin{array}{l}[(A_j)_{1,2}/(\sigma_n DC_{j1})(\sigma_n DC_{j2})] + [(A_j)_{2,3}/(\sigma_n DC_{j2})(\sigma_n DC_{j3})] + \\ [(A_j)_{3,4}/(\sigma_n DC_{j3})(\sigma_n DC_{j4})] + [(A_j)_{1,3}/(\sigma_n DC_{j1})(\sigma_n DC_{j3})] + \\ [(A_j)_{1,4}/(\sigma_n DC_{j1})(\sigma_n DC_{j4})] + [(A_j)_{2,4}/(\sigma_n DC_{j2})(\sigma_n DC_{j4})]\end{array}}{\dfrac{1}{\begin{array}{l}[(\sigma_n DC_{j1})(\sigma_n DC_{j2}) + (\sigma_n DC_{j2})(\sigma_n DC_{j3}) + (\sigma_n DC_{j3})(\sigma_n DC_{j4}) + \\ (\sigma_n DC_{j1})(\sigma_n DC_{j3}) + (\sigma_n DC_{j1})(\sigma_n DC_{j4}) + (\sigma_n DC_{j2})(\sigma_n DC_{j4})]\end{array}}}$$

When all the field decay powers have been calculated, the Fourier coefficients are normalized using their respective magnetometer radii and field decay powers to produce magnetic field modeling coefficients, These field modeling coefficients are a result of a weighted average of each set of Fourier coefficients over all four magnetometers using their respective normalized standard deviations to provide the weighting factors:

$$C_j n = \sum_{i=1}^{4}(C_j n_i (R_i)^{Bn_j}/\sigma_n C_j n_i)/\sum_{i=1}^{4} 1/\sigma_n C_j n_i$$
$$S_j n = \sum_{i=1}^{4}(S_j n_i (R_i)^{Cn_j}/\sigma_n S_j n_i)/\sum_{i=1}^{4} 1/\sigma_n S_j n_i$$
$$DC_j = \sum_{i=1}^{4}(DC_{ji} (R_i)^{A_j}/\sigma_n DC_{ji})/\sum_{i=1}^{4} 1/\sigma_n DC_{ji}$$

Where:

$C_j n$ = cosine field modeling coefficient calculated for n = 1 to 4;
$S_j n$ = sine field modeling coefficient calculated for n = 1 to 4; and
$DC_j$ = constant field (Z-axis) modeling coefficient.

## Magnetic Field Modeling Equation

Finally, the field modeling coefficients and field decay powers are used in the magnetic field modeling equation. This equation reconstructs the three components of the magnetic field on the X-Y plane of the magnetometers as a function of radial distance from the center of rotation (R) and the angle of rotation ($\theta$).

$$B_j(R,\theta) = DC_j / R^{A_j} + \sum_{n=1}^{4}(C_j n)\cos(n\theta) / R^{B_{n_j}} + \sum_{n=1}^{4}(S_j n)\sin(n\theta) / R^{C_{n_j}}$$

Assuming four triaxial magnetometers are used in the dipole moment measurements (i = 1 to 4), the components (for n=4) from the X-axis magnetometers are:

$$CX_i = (2A_{11}/R_i^3 - 6A_{31}/R_i^5 + 45A_{51}/4R_i^7 - 35A_{71}/2R_i^9)$$

$$SX_i = (2B_{11}/R_i^3 - 6B_{31}/R_i^5 + 45B_{51}/4R_i^7 - 35B_{71}/2R_i^9)$$

The components from the Y-axis magnetometers are:

$$CY_i = -(B_{11}/R_i^3 - 3B_{31}/2R_i^5 + 15B_{51}/8R_i^7 - 35B_{71}/16R_i^9)$$

$$SY_i = (A_{11}/R_i^3 - 3A_{31}/2R_i^5 + 15A_{51}/8R_i^7 - 35A_{71}/16R_i^9)$$

The constant component from the Z-axis magnetometers is:

$$DCZ_i = -(A_{10}/R_i^3 - 3A_{30}/2R_i^5 + 15A_{50}/8R_i^7 - 35A_{70}/16R_i^9)$$

Where:

| | |
|---|---|
| $A_{11}$ | = X-axis dipole moment coefficient; |
| $A_{31}, A_{51}, A_{71}$ | = Contributions to the fundamental component from the X-axis multi-pole (octapole, etc.) moments; |
| $B_{11}$ | = Y-axis dipole moment coefficient; |
| $B_{31}, B_{51}, B_{71}$ | = Contributions to the fundamental component from the Y-axis multi-pole (octapole, etc.) moments; |
| $A_{10}$ | = Z-axis dipole moment coefficient; and |
| $A_{30}, A_{50}, A_{70}$ | = Contributions to the constant component from the Z-axis multi-pole (octapole, etc.) moments. |

The Fourier analysis equations to measure the fundamental and constant components from rotational magnetic field data taken every 10° are:

$$CX_i = \tfrac{1}{\pi}\int_0^{2\pi} B_x(R_i,\theta)\cos\theta\, d\theta = \tfrac{1}{18}\sum_{\theta=0°}^{360°} B_x(R_i,\theta)\cos\theta$$

$$SX_i = \tfrac{1}{\pi}\int_0^{2\pi} B_x(R_i,\theta)\sin\theta\, d\theta = \tfrac{1}{18}\sum_{\theta=0°}^{360°} B_x(R_i,\theta)\sin\theta$$

$$CY_i = \tfrac{1}{\pi}\int_0^{2\pi} B_y(R_i,\theta)\cos\theta\, d\theta = \tfrac{1}{18}\sum_{\theta=0°}^{360°} B_y(R_i,\theta)\cos\theta$$

$$SY_i = \tfrac{1}{\pi}\int_0^{2\pi} B_y(R_i,\theta)\sin\theta\, d\theta = \tfrac{1}{18}\sum_{\theta=0°}^{360°} B_y(R_i,\theta)\sin\theta$$

$$DCZ_i = \tfrac{1}{2\pi}\int_0^{2\pi} B_z(R_i,\theta)\, d\theta = \tfrac{1}{36}\sum_{\theta=0°}^{360°} B_z(R_i,\theta)$$

Where:

| | |
|---|---|
| $B_x, B_y, B_z$ | = X-, Y- and Z-axis magnetic fields (nT); |
| $R_i$ | = Magnetometer radial distance (m); |
| $\theta$ | = Rotation angle; and |
| i | = Magnetometer number, 1 to 4. |

## X Moment Near-Field Analysis

The X Moment Fourier coefficient and Near Field matrices are as follows:

$$
\begin{vmatrix} \dfrac{CX_i}{\sigma CX_i} \\[2mm] \dfrac{SY_i}{\sigma SY_i} \\[2mm] |Q\,Matrix| \end{vmatrix}
=
\begin{vmatrix} \dfrac{2(R_1/R_i)^3}{\sigma CX_i} & \dfrac{-6(R_1/R_i)^5}{\sigma CX_i} & \dfrac{45(R_1/R_i)^7}{4\sigma CX_i} & \dfrac{-35(R_1/R_i)^9}{2\sigma CX_i} \\[2mm] \dfrac{(R_1/R_i)^3}{\sigma SY_i} & \dfrac{-3(R_1/R_i)^5}{2\sigma SY_i} & \dfrac{15(R_1/R_i)^7}{8\sigma SY_i} & \dfrac{-35(R_1/R_i)^9}{16\sigma SY_i} \\[2mm] column_1 & column_2 & column_3 & column_4 \end{vmatrix}
\times
\begin{vmatrix} A_{11} \\ A_{31} \\ A_{51} \\ A_{71} \end{vmatrix}
$$

Solving for the Data Matrix results in the following:

$$DM_1 = \sum Q\,Matrix \times column_1 = \sum (R_1/R_i)^3 \times \left(2CX_i/(\sigma CX_i)^2 + SY_i/(\sigma SY_i)^2\right)$$

$$DM_2 = \sum Q\,Matrix \times column_2 = \sum (R_1/R_i)^5 \times \left(-6CX_i/(\sigma CX_i)^2 - 3SY_i/2(\sigma SY_i)^2\right)$$

$$DM_3 = \sum Q\,Matrix \times column_3 = \sum (R_1/R_i)^7 \times \left(45CX_i/4(\sigma CX_i)^2 + 15SY_i/8(\sigma SY_i)^2\right)$$

$$DM_4 = \sum Q\,Matrix \times column_4 = \sum (R_1/R_i)^9 \times \left(-35CX_i/2(\sigma CX_i)^2 - 35SY_i/16(\sigma SY_i)^2\right)$$

Solving for the Measurement Matrix results in the following:

$$MM_{11} = \sum (column_1)^2 = \sum (R_1/R_i)^6 \times \left((2/\sigma CX_i)^2 + (1/\sigma SY_i)^2\right)$$

$$MM_{22} = \sum (column_2)^2 = \sum (R_1/R_i)^{10} \times \left((-6/\sigma CX_i)^2 + (-3/2\sigma SY_i)^2\right)$$

$$MM_{33} = \sum (column_3)^2 = \sum (R_1/R_i)^{14} \times \left((45/4\sigma CX_i)^2 + (15/8\sigma SY_i)^2\right)$$

$$MM_{44} = \sum (column_4)^2 = \sum (R_1/R_i)^{18} \times \left((-35/2\sigma CX_i)^2 + (-35/16\sigma SY_i)^2\right)$$

$$MM_{12} = MM_{21} = \sum (column_1) \times (column_2) = \sum (R_1/R_i)^8 \times \left(-12/(\sigma CX_i)^2 - 3/2(\sigma SY_i)^2\right)$$

$$MM_{13} = MM_{31} = \sum (column_1) \times (column_3) = \sum (R_1/R_i)^{10} \times \left(90/4(\sigma CX_i)^2 + 15/8(\sigma SY_i)^2\right)$$

$$MM_{14} = MM_{41} = \sum (column_1) \times (column_4) = \sum (R_1/R_i)^{12} \times \left(-70/2(\sigma CX_i)^2 - 35/16(\sigma SY_i)^2\right)$$

$$MM_{23} = MM_{32} = \sum (column_2) \times (column_3) = \sum (R_1/R_i)^{12} \times \left(-270/4(\sigma CX_i)^2 - 45/16(\sigma SY_i)^2\right)$$

$$MM_{24} = MM_{42} = \sum (column_2) \times (column_4) = \sum (R_1/R_i)^{14} \times \left(210/2(\sigma CX_i)^2 + 105/32(\sigma SY_i)^2\right)$$

$$MM_{34} = MM_{43} = \sum (column_3) \times (column_4) = \sum (R_1/R_i)^{16} \times \left(-1575/8(\sigma CX_i)^2 - 525/128(\sigma SY_i)^2\right)$$

Thus, solving for the dipole moments requires the following matrix:

$$\begin{vmatrix} DM_1 \\ DM_2 \\ DM_3 \\ DM_4 \end{vmatrix} = \begin{vmatrix} MM_{11} & MM_{21} & MM_{31} & MM_{41} \\ MM_{12} & MM_{22} & MM_{32} & MM_{42} \\ MM_{13} & MM_{23} & MM_{33} & MM_{43} \\ MM_{14} & MM_{24} & MM_{34} & MM_{44} \end{vmatrix} \times \begin{vmatrix} A_{11} \\ A_{31} \\ A_{51} \\ A_{71} \end{vmatrix}$$

For the first iteration dipole moment calculation (N=1), a 1x1 matrix is produced that reveals dipole fields only. Solving for the dipole moment:

$$Moment = A_{11} \times 10\,R_1^3$$

$$Moment = (DM1/MM_{11}) \times 10\,R_1^3$$

For the second iteration dipole moment calculation (N=2), a 2x2 matrix is produced that reveals dipole and octapole fields. Solving for the dipole moment:

$$Moment = \frac{DM1*MM22 - DM2*MM21}{MM11*MM22 - MM12*MM21} \times 10\,R_1^3$$

For the third iteration dipole moment calculation (N=3), a 3x3 matrix is produced that reveals higher order multipole fields. Solving for the dipole moment:

$$Moment = \frac{\begin{aligned} &DM_1 \times (MM_{22} \times MM_{33} - MM_{23} \times MM_{32}) - \\ &MM_{21} \times (DM_2 \times MM_{33} - DM_3 \times MM_{32}) + \\ &MM_{31} \times (DM_2 \times MM_{23} - DM_3 \times MM_{22}) \end{aligned}}{\begin{aligned} &MM_{11} \times (MM_{22} \times MM_{33} - MM_{23} \times MM_{32}) - \\ &MM_{21} \times (MM_{12} \times MM_{33} - MM_{13} \times MM_{32}) + \\ &MM_{31} \times (MM_{12} \times MM_{23} - MM_{13} \times MM_{22}) \end{aligned}} \times 10\,R_1^3$$

*Y Moment Near-Field Analysis*

Solving for the Y Moment Data Matrix results in the following:

$$DM_1 = \sum (R_1/R_i)^3 \times \left(2SX_i/(\sigma SX_i)^2 - CY_i/(\sigma CY_i)^2\right)$$

$$DM_2 = \sum (R_1/R_i)^5 \times \left(-6SX_i/(\sigma SX_i)^2 + 3CY_i/2(\sigma CY_i)^2\right)$$

$$DM_3 = \sum (R_1/R_i)^7 \times \left(45SX_i/4(\sigma SX_i)^2 - 15CY_i/8(\sigma CY_i)^2\right)$$

$$DM_4 = \sum (R_1/R_i)^9 \times \left(-35SX_i/2(\sigma SX_i)^2 + 35CY_i/16(\sigma CY_i)^2\right)$$

Solving for the Measurement Matrix results in the following:

$$MM_{11} = \sum (R_1/R_i)^6 \times \left((2/\sigma SX_i)^2 + (1/\sigma CY_i)^2\right)$$

$$MM_{22} = \sum (R_1/R_i)^{10} \times \left((-6/\sigma SX_i)^2 + (-3/2\sigma CY_i)^2\right)$$

$$MM_{33} = \sum (R_1/R_i)^{14} \times \left((45/4\sigma SX_i)^2 + (15/8\sigma CY_i)^2\right)$$

$$MM_{44} = \sum (R_1/R_i)^{18} \times \left((-35/2\sigma SX_i)^2 + (-35/16\sigma CY_i)^2\right)$$

$$MM_{12} = MM_{21} = \sum (R_1/R_i)^8 \times \left(-12/(\sigma SX_i)^2 - 3/2(\sigma CY_i)^2\right)$$

$$MM_{13} = MM_{31} = \sum (R_1/R_i)^{10} \times \left(90/4(\sigma SX_i)^2 + 15/8(\sigma CY_i)^2\right)$$

$$MM_{14} = MM_{41} = \sum (R_1/R_i)^{12} \times \left(-70/2(\sigma SX_i)^2 - 35/16(\sigma CY_i)^2\right)$$

$$MM_{23} = MM_{32} = \sum (R_1/R_i)^{12} \times \left(-270/4(\sigma SX_i)^2 - 45/16(\sigma CY_i)^2\right)$$

$$MM_{24} = MM_{42} = \sum (R_1/R_i)^{14} \times \left(210/2(\sigma SX_i)^2 + 105/32(\sigma CY_i)^2\right)$$

$$MM_{34} = MM_{43} = \sum (R_1/R_i)^{16} \times \left(-1575/8(\sigma SX_i)^2 - 525/128(\sigma CY_i)^2\right)$$

The Y Moment is calculated using moment equations for the X-axis.

*Z Moment Near-Field Analysis*

Solving for the Z Moment Data Matrix results in the following:

$$DM_1 = \sum (R_1/R_i)^3 \times \left(-DCZ_i/(\sigma DCZ_i)^2\right)$$

$$DM_2 = \sum (R_1/R_i)^5 \times \left(3DCZ_i/2(\sigma DCZ_i)^2\right)$$

$$DM_3 = \sum (R_1/R_i)^7 \times \left(-15DCZ_i/8(\sigma DCZ_i)^2\right)$$

$$DM_4 = \sum (R_1/R_i)^9 \times \left(35DCZ_i/16(\sigma DCZ_i)^2\right)$$

Solving for the Measurement Matrix results in the following:

$$MM_{11} = \sum (R_1/R_i)^6 \times (1/\sigma DCZ_i)^2$$

$$MM_{22} = \sum (R_1/R_i)^{10} \times (-3/2\sigma DCZ_i)^2$$

$$MM_{33} = \sum (R_1/R_i)^{14} \times (15/8\sigma DCZ_i)^2$$

$$MM_{44} = \sum (R_1/R_i)^{18} \times (-35/16\sigma DCZ_i)^2$$

$$MM_{12} = MM_{21} = \sum (R_1/R_i)^8 \times \left(-3/2(\sigma DCZ_i)^2\right)$$

$$MM_{13} = MM_{31} = \sum (R_1/R_i)^{10} \times \left(15/8(\sigma DCZ_i)^2\right)$$

$$MM_{14} = MM_{41} = \sum (R_1/R_i)^{12} \times \left(-35/16(\sigma DCZ_i)^2\right)$$

$$MM_{23} = MM_{32} = \sum (R_1/R_i)^{12} \times \left(-45/16(\sigma DCZ_i)^2\right)$$

$$MM_{24} = MM_{42} = \sum (R_1/R_i)^{14} \times \left(105/32(\sigma DCZ_i)^2\right)$$

$$MM_{34} = MM_{43} = \sum (R_1/R_i)^{16} \times \left(-525/128(\sigma DCZ_i)^2\right)$$

The Z Moment is calculated using moment equations for the X-axis.

The $\sigma CX_i$, $\sigma SY_i$, $\sigma SX_i$, $\sigma CY_i$ and $\sigma DCZ_i$ variables are moment constant term standard deviations derived from the average data values calculated based on five rotational runs. Experience has shown that only one rotational run is necessary. Since only one rotational run is used, the standard deviation values are equal to 1 and drop out of the dipole moment calculations used in the LabVIEW rotational data analysis software.

## Discussion

The magnetic field dipole moment modeling technique has been implemented on a microcomputer-controlled data acquisition and analysis system at the Goddard Space Flight Center Magnetic Test Facility. This system is described in [2] and consists of National Instruments (NI) hardware and NI LabVIEW software. The hardware includes a NI plug-in data acquisition board inside the microcomputer (or a data acquisition card in a laptop) cabled to an external Signal Conditioning eXtensions for Instrumentation (SCXI) chassis with signal SCXI conditioning equipment. LabVIEW is an object-oriented graphic programming code used for data acquisition, analysis and presentation.

The basic assumption that Fourier coefficients have the same polarity for all magnetometers and decrease with increasing radius leads to certain spatial limitations of the technique. In the extreme near-field region, complex magnetic sources with higher order multi-pole moments can overshadow lower order moment contributions to the Fourier coefficients. This condition allows the possibility of polarity reversals with decreasing radius. Therefore, to maximize accuracy, the region to be modeled should be narrowly defined by the placement of in measurement magnetometers around complex magnetic sources.

The possible calculation of total field, three-dimensional magnetic field models is offered by rotating the spacecraft and acquiring data for different values of the vertical angle $\varphi$, from 0 to $\pi$. This provides data for models on R-$\theta$ planes as a function of $\varphi$, allowing modeling on R-$\varphi$ planes as a continuous function of $\theta$. This would yield coefficients sufficient to provide modeling over all R, $\theta$ and $\varphi$ parameters; however, it is felt that most modeling requirements could be met with simple mapping on a single R-$\theta$ plane or over just a limited region of the vertical angle.

## Conclusions

Test results obtained from modeling magnetic fields around several different spacecraft and flight experiments indicate that the magnetic field modeling technique, combined with a computer-controlled measure system, provides capability for complex magnetic dipole moment analysis. Modeling accuracy is sufficient to provide detailed analysis of complex magnetic sources, even where field levels are less than 1.0 nT.

Presentation of the magnetic dipole moment model can he achieved in real-time, using high-speed data acquisition and analysis augmented by a CRT and laser printer. Similar systems have been incorporated into existing magnetic measurement facilities and also could be designed as part of the spacecraft checkout platform on the Space Shuttle. Magnetic testing using the Shuttle would allow measurements to be made on spacecraft operating in true flight configurations, significantly increasing the reliability and utility of the data.

## References

1. Eichhorn, William I. (1972), "Magnetic Dipole Moment Determination by Near-Field Analysis," *NASA Technical Note D-6685*.

2. Harris, Patrick K. (1999), "Management Of Automated Systems: Proper Planning To Enhance Work Performance," Kennedy-Western University.